Local spectrum analysis of field propagation in an anisotropic medium. Part I. Time-harmonic fields

Igor Tinkelman and Timor Melamed

Department of Electrical and Computer Engineering, Ben-Gurion University of the Negev, Beer Sheva 84105, Israel

Received October 14, 2004; accepted December 11, 2004

The phase-space beam summation is a general analytical framework for local analysis and modeling of radiation from extended source distributions. In this formulation, the field is expressed as a superposition of beam propagators that emanate from all points in the source domain and in all directions. In this Part I of a two-part investigation, the theory is extended to include propagation in anisotropic medium characterized by a generic wave-number profile for time-harmonic fields; in a companion paper [J. Opt. Soc. Am. A **22**, 1208 (2005)], the theory is extended to time-dependent fields. The propagation characteristics of the beam propagators in a homogeneous anisotropic medium are considered. With use of Gaussian windows for the local processing of either ordinary or extraordinary electromagnetic field distributions, the field is represented by a phase-space spectral distribution in which the propagating elements are Gaussian beams that are formulated by using Gaussian plane-wave spectral distributions over the extended source plane. By applying saddle-point asymptotics, we extract the Gaussian beam phenomenology in the anisotropic environment. The resulting field is parameterized in terms of the spatial evolution of the beam curvature, beam width, etc., which are mapped to local geometrical properties of the generic wave-number profile. The general results are applied to the special case of uniaxial crystal, and it is found that the asymptotics for the Gaussian beam propagators, as well as the physical phenomenology attached, perform remarkably well.

OCIS codes: 350.5500, 260.1180.

1. INTRODUCTION

Phase-space (PS) spectral representations, in which the spectral elements are beams (or pulsed beams for time-dependent fields), have been the subject of intense research in the past decade, owing to their spectral localization and the capability of propagating theseAu: Please clarify if not correct spectral wave objects in complex environments. In contrast, conventional wave elements such as Green's functions or plane waves are hard to track in inhomogeneous environments or through interactions with objects, and the resulting spectral integrals are spectrally distributed.

Several PS expansion schemes for wave propagation have been introduced for extended source configurations; these schemes use a spectrum of shifted and tilted beams that emanate in all directions from all points in the source domain.[1–4] In Refs. 2,4 and 5 these schemes have been placed within a unified PS format wherein a PS distribution of beam propagators is locally matched to the source distribution. Recently discrete PS spectral representations based on the discrete Wilson basis[6] and on frame theory[7] have been introduced.

In the present contribution, the PS continuance spectral representation for time-harmonic excitation, which was originally introduced in Ref. 2, is extended to include propagation in an anisotropic medium characterized by a generic wave-number profile for both time-harmonic and, in the companion paper,[8] for time-dependent fields. Anisotropic materials are of interest for optical waveguides, microwave devices, plasma science, and different propagation environments. Comprehensive studies have been conducted on the problem of Gaussian beam (GB) two- and three-dimensional propagation for specific wave-number profiles[9–14] as well as on modeling different types of anisotropic propagation and scattering[15,16] with GBs as basis wave objects. Nevertheless, to our knowledge, the propagation of GBs in a *generic* anisotropic medium has not yet been explored in detail. In Ref. 17, using the complex source method, the authors arrived at a closed-form analytic solution for the GB field. In our view, the complex source method cannot account for the astigmatic effects that are present in our analysis of the generic wave-number profile, and therefore these results may be applied only to the case of GB propagation along the optical axis of a uniaxially anisotropic medium. Alternatively, by applying a plane-wave spectral representation to the propagation problem, in Ref. 18 we have presented an alternative rigorous solution for the GB field for the case of a nontilted GB. In the current paper, this preliminary investigation is placed within the framework of the Gaussian beam summation method to include generally tilted beam solutions and their parameterization, novel phase-space phenomenologies related to the generic anisotropy characteristics, and extension to the time domain.[8]

2. FORMULATION

The current study is concerned with the effects of anisotropy on the propagation characteristics of either an electromagnetic or a general linear field in a lossless homoge-

neous medium. The field is formulated by means of its initial distribution over the $z=0$ plane by use of the conventional Cartesian coordinate system $\mathbf{r}=(\mathbf{x},z)$ with $\mathbf{x}=(x_1,x_2)$. In an anisotropic medium, exact field representations may be constructed by use of the eigenfunction expansion,[19] usually in the form of a plane-wave spectral integral. The latter consist of ordinary and extraordinary modes, whose distributions are determined by matching the plane-wave spectral distributions to a specific source distribution (see examples in Refs. 19 and 20). With this procedure, the vectorial problem is reduced to scalar field propagation of ordinary and extraordinary distributions. The initial field distribution over the $z=0$ plane (of any of the anisotropic modes of propagation) is denoted $\hat{u}_o(\mathbf{x})$, where here and henceforth a caret denotes time-harmonic field constituents with $\exp(-i\omega t)$ time dependence assumed and suppressed, so that $\hat{u}_o(\mathbf{x})=\hat{u}_o(\mathbf{x},\omega)$, etc. The lossless propagation medium is characterized by a generic wave-number profile, in which the longitudinal wave number in the direction of the z axis is a function of the (plane-wave) direction of propagation, $k_z=k_z(k_{x_1},k_{x_2})$, where (k_{x_1},k_{x_2}) is the wave-number vector in the $\mathbf{x}=(x_1,x_2)$ direction. Anticipating extension to the time domain (see Part II[8]), we normalize the wave numbers by the isotropic wave number $k_o=\omega/c$, with c being a constant. The constant c may be chosen as the speed of light *in vacuo* or any other constant [see, for example, the uniaxial crystal wave-number profile in Eqs. (53) and (54)]. Therefore the medium anisotropy may be characterized by the normalized longitudinal wave number $\zeta(\boldsymbol{\xi})$

$$\zeta(\boldsymbol{\xi})=k_z(k_{x_1},k_{x_2})/k_o,\quad k_o=\omega/c,$$

$$\boldsymbol{\xi}=(k_{x_1},k_{x_2})/k_o, \tag{1}$$

and the field may be propagated away from the $z=0$ plane by use of the anisotropic plane-wave propagator $\exp[ik_z(k_{x_1},k_{x_2})z]=\exp[ik_o\zeta(\boldsymbol{\xi})z]$.

A. Space–Wave-Number Transforms

The frequency domain wave-number spectral distribution over the initial $z=0$ plane is defined by the two-dimensional spatial Fourier transform

$$\hat{\tilde{u}}_o(\boldsymbol{\xi})=\int_{-\infty}^{\infty}\mathrm{d}^2x\hat{u}_o(\mathbf{x})\exp(-ik_o\boldsymbol{\xi}\cdot\mathbf{x}), \tag{2}$$

where $\boldsymbol{\xi}=(\xi_1,\xi_2)$ is the normalized spatial wave-number vector, $\mathbf{x}=(x_1,x_2)$, and the tilde identifies a wave-number spectral function. The reconstruction of the frequency-domain initial field is, accordingly,

$$\hat{u}_o(\mathbf{x})=\left(\frac{k_o}{2\pi}\right)^2\int\mathrm{d}^2\xi\hat{\tilde{u}}_o(\boldsymbol{\xi})\exp(ik_o\boldsymbol{\xi}\cdot\mathbf{x}). \tag{3}$$

The normalization with respect to k_o anticipates inversion to the time domain (see Part II[8]), rendering $\boldsymbol{\xi}$ frequency independent, with direct geometrical interpretation in terms of the spectral plane-wave propagation angles. For simplicity, integration limits are omitted on all integrals extending from $-\infty$ to $+\infty$.

Using the anisotropic propagator in Eq. (1) and assuming that all sources are located in $z<0$, the field propagating into $z>0$ half-space is given by

$$\hat{u}(\mathbf{r})=\left(\frac{k_o}{2\pi}\right)^2\int\mathrm{d}^2\xi\hat{\tilde{u}}_o(\boldsymbol{\xi})\exp[ik_o(\boldsymbol{\xi}\cdot\mathbf{x}+\zeta(\boldsymbol{\xi})z)]. \tag{4}$$

Equation (4) reconstructs the field in terms of angular ($\boldsymbol{\xi}$) superposition of a plane wave propagating in the direction of the unit vector:

$$\hat{\boldsymbol{\kappa}}(\boldsymbol{\xi})=[\boldsymbol{\xi},\zeta(\boldsymbol{\xi})]/[\boldsymbol{\xi}^2+\zeta^2(\boldsymbol{\xi})]^{1/2},\quad \boldsymbol{\xi}^2=\boldsymbol{\xi}\cdot\boldsymbol{\xi}. \tag{5}$$

The plane-wave integrals in Eq. (4) are spectrally distributed. For high-frequency signals, however, dominant contributions are generated by localized regions in the source domain that emphasizes radiation in a given direction. We assume that the source distribution has the high-frequency form (the so-called Lagrange manifold),

$$u_o(\mathbf{x})=A_o(\mathbf{x})\exp[ik_o\Phi_o(\mathbf{x})], \tag{6}$$

where $A_o(\mathbf{x})$ is the amplitude and $\Phi_o(\mathbf{x})$ is a phase function, both with slow spatial $\mathbf{x}$ variation. For high-frequency distribution of the form of Eq. (6), the dominant contribution to the plane-wave spectrum in Eq. (2) comes from the region of the stationary point $\mathbf{x}_s(\boldsymbol{\xi})$, defined by

$$\nabla\Phi_o(\mathbf{x})=\boldsymbol{\xi},\quad \text{at } \mathbf{x}_s(\boldsymbol{\xi}). \tag{7}$$

For a given $\mathbf{x}$, this condition defines the local radiation direction if a plane wave is locally matched to the source distribution. A ray-field representation may be obtained by asymptotically evaluating Eq. (4), using the asymptotic spectral distribution. In this representation, a ray is emanating from each point $\mathbf{x}$ in the aperture in a direction $\hat{\boldsymbol{\kappa}}(\boldsymbol{\xi}=\boldsymbol{\xi}_s)$ of Eq. (5), where the stationary ray $\boldsymbol{\xi}_s$ satisfies Eq. (7) for a given $\mathbf{x}$.

We shall not go through the complete asymptotic manipulations here, as our goal is not to derive analytic ray-type local approximations. Instead, in Subsections 2.B and 2.C we shall show how local PS transforms yield spectral representations that are *a priori* localized about the ray skeleton defined by Eq. (7).

B. Phase-Space Processing

In this subsection we summarize the PS analysis and synthesis formalisms that parameterize the field over the $z=0$ initial plane (further details may be found in Ref. 4) as well as formulate the PS anisotropic beam propagators. We shall use a continuous spectral representation [see Ref. (12)], but the theory presented here may be used for discrete frame-based representation, provided that the overcompleteness frame parameter is larger than 0.45, since under this condition, the local PS propagators that are presented and analyzed here coincide with those obtained by the discrete representation.[7] For the desired local spectral analysis of the field distribution, we generate the local (plane-wave) spectrum by means of a windowed Fourier transform of the distribution in configuration space,

$$\hat{U}_o(\bar{\mathbf{X}})=\int\mathrm{d}^2x\hat{u}_o(\mathbf{x})\hat{W}^*(\mathrm{x};\bar{\mathbf{X}}),$$

$$\hat{W}(\mathbf{x};\bar{\mathbf{X}}) = \hat{w}(\mathbf{x}-\bar{\mathbf{x}})\exp[ik_o\bar{\boldsymbol{\xi}}\cdot(\mathbf{x}-\bar{\mathbf{x}})], \tag{8}$$

where the asterisk denotes the complex conjugate and $\bar{\mathbf{X}} = (\bar{\mathbf{x}}, \bar{\boldsymbol{\xi}})$. Here, $\hat{w}(\mathbf{x})$ is a spatial window function, centered at $\bar{\mathbf{x}} = (\bar{x}_1, \bar{x}_2)$ with linear phasing specified by $\bar{\boldsymbol{\xi}} = (\bar{\xi}_1, \bar{\xi}_2)$. The vector $\bar{\mathbf{X}}$ incorporates the configuration-spectrum PS coordinates $(\bar{\mathbf{x}}, \bar{\boldsymbol{\xi}})$, whence $\hat{U}_o(\bar{\mathbf{X}})$ is referred to as a PS distribution of the initial field distribution $\hat{u}_o(\mathbf{x})$. Transform (8) extracts from $\hat{u}_o(\mathbf{x})$ the local spectrum around the $\bar{\boldsymbol{\xi}}$-directed propagation at the window center $\bar{\mathbf{x}}$ (see Fig. 1). In typical propagation and scattering problems, the spectrum at a given $\bar{\mathbf{x}}$ is localized about a preferred spectral direction $\bar{\boldsymbol{\xi}}(\bar{\mathbf{x}})$ that describes the (stationary) direction of propagation of the incident field at $\bar{\mathbf{x}}$ point (the Lagrange manifold). Consequently, the local spectrum $\hat{U}_o(\bar{\mathbf{X}})$ is localized *a priori* about the subdomain $(\bar{\mathbf{x}}, \bar{\boldsymbol{\xi}}) = [\bar{\mathbf{x}}, \bar{\boldsymbol{\xi}}(\bar{\mathbf{x}})]$ in the $\bar{\mathbf{X}}$ domain (see synthetic examples in Refs. 2,4). In the present context of anisotropic propagation, where $\hat{u}_o(\mathbf{x})$ is either ordinary- or extraordinary-mode distribution, it is convenient to describe the local spectrum by the initial plane-wave distribution that is obtained by matching to the source plane-wave representation. By inserting Eq. (3) into Eq. (8) and inverting the order of integration, we obtain

$$\hat{U}_o(\bar{\mathbf{X}}) = (k_o/2\pi)^2 \int \mathrm{d}^2\xi \hat{\tilde{u}}_o(\boldsymbol{\xi})\hat{\tilde{W}}^*(\boldsymbol{\xi};\bar{\mathbf{X}}),$$

$$\hat{\tilde{W}}(\boldsymbol{\xi};\bar{\mathbf{X}}) = \hat{\tilde{w}}(\boldsymbol{\xi}-\bar{\boldsymbol{\xi}})\exp(-ik_o\boldsymbol{\xi}\cdot\bar{\mathbf{x}}), \tag{9}$$

with $\hat{\tilde{W}}$ and $\hat{\tilde{w}}$ being the wave-number spectra (2) of $\hat{W}$ and $\hat{w}$, respectively.

The field distribution $\hat{u}_o(\mathbf{x})$ may be synthesized from its PS spectrum through the inverse PS transform[4]

$$\hat{u}_o(\mathbf{x}) = \left(\frac{k_o}{2\pi\hat{N}}\right)^2 \int \mathrm{d}^4\bar{X}\hat{U}_o(\bar{\mathbf{X}})\hat{W}(\mathbf{x};\bar{\mathbf{X}}), \tag{10}$$

where

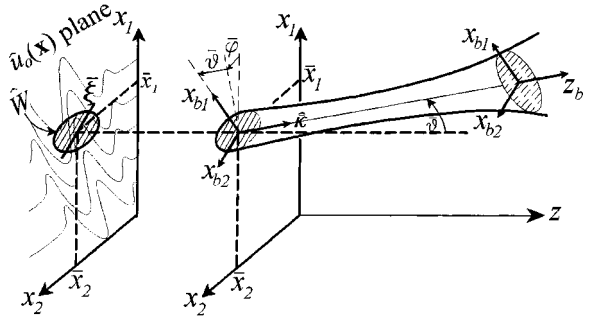

Fig. 1. Local processing of the time-harmonic field distribution; the PS distribution $\hat{U}_o(\bar{\mathbf{X}})$ is obtained by integrating the field distribution $\hat{u}_o(\mathbf{x})$ with a linearly phased window function shifted to point $\bar{\mathbf{x}}$. The linear phase extracts from $\hat{u}_o$ its local directional properties and by that matches a single beam propagator emanating from the window center at $\bar{\mathbf{x}}$ along the (ordinary) direction identified by the spherical angles $(\bar{\vartheta}, \bar{\varphi})$.

$$\hat{N} = \left[\int \mathrm{d}^2x|\hat{w}(\mathbf{x})|^2\right]^{1/2} \tag{11}$$

is the $\mathcal{L}^2_{\mathbf{x}}$ norm of $\hat{w}$. With use of inverse transform (10), the PS superposition of the initial field can be propagated into $z>0$, giving

$$\hat{u}(\mathbf{r},\omega) = \left(\frac{k_o}{2\pi\hat{N}}\right)^2 \int \mathrm{d}^4\bar{X}\hat{U}_o(\bar{\mathbf{X}})\hat{B}(\mathbf{r};\bar{\mathbf{X}}), \tag{12}$$

where $\hat{N}$ is given in Eq. (11) and the PS propagator $\hat{B}$ is the field that is radiated by each PS window element $\hat{W}(\mathbf{x};\bar{\mathbf{X}})$ in Eq. (10). For anisotropic propagation, it is convenient to express the PS propagators by a plane-wave representation, i.e.,

$$\hat{B}(\mathbf{r};\bar{\mathbf{X}}) = \left(\frac{k_o}{2\pi}\right)^2 \int \mathrm{d}^2\xi\hat{\tilde{W}}(\boldsymbol{\xi};\bar{\mathbf{X}})\exp[ik_o(\boldsymbol{\xi}\cdot\mathbf{x}+\zeta(\boldsymbol{\xi})z)], \tag{13}$$

where the plane-wave spectrum $\hat{\tilde{W}}$ is given in Eqs. (9). If $\hat{w}$ is wide on a wavelength scale, then the spatial and spectral distributions of $\hat{W}$ are localized around $\mathbf{x}=\bar{\mathbf{x}}$ and $\boldsymbol{\xi}=\bar{\boldsymbol{\xi}}$, respectively, and consequently, $\hat{B}$ behaves as a collimated beam [see Eqs. (19) and (40) for ordinary and extraordinary GBs, respectively]. The representation in Eq. (12) describes the radiated field as a continuous superposition of shifted and tilted beams, centered at and directed along $\bar{\mathbf{x}}$ and $\bar{\boldsymbol{\xi}}$, respectively. The PS function $\hat{U}_o(\bar{\mathbf{X}})$ defines the excitation strengths of these beams through local matching to the aperture field $\hat{u}_o(\mathbf{x})$ (see Fig. 1).

C. Gaussian Windows

Next we examine the special case of Gaussian windows. These have been used extensively for modeling beam propagation since they maximize the PS localization as implied by the uncertainty principle and yield analytically trackable beam-type propagators.[2,4,7,21,22] For locally (PS) processing the field distribution, we use a Gaussian window whose spatial and spectral distributions are

$$\hat{w}(\mathbf{x}) = \exp\left(\frac{i}{2}k_o\mathbf{x}\boldsymbol{\Gamma}\mathbf{x}^T\right),$$

$$\hat{\tilde{w}}(\boldsymbol{\xi}) = \frac{2\pi i}{k_o\Gamma}\exp\left(-\frac{i}{2}k_o\boldsymbol{\xi}\boldsymbol{\Gamma}^{-1}\boldsymbol{\xi}^T\right), \tag{14}$$

with $\boldsymbol{\Gamma}=\Gamma\mathbf{I}$, where $\mathbf{I}$ is the unity matrix and $\Gamma=\Gamma_r+i\Gamma_i$ is the window complex parameter with $\Gamma_i>0$. Anticipating extension to the time domain, we have constructed definition (14) so that the frequency $k_o=\omega/c$ appears explicitly in the exponent and Γ is frequency independent (see also the discussion in Part II,[8] Subsection 1.D). In Eqs. (14), $\mathbf{x}=(x_1,x_2)$ is a line vector and T denotes the transpose vector, so that the window exponent takes the quadratic form $\mathbf{x}\boldsymbol{\Gamma}\mathbf{x}^T=\Gamma(x_1^2+x_2^2)$. The $\boldsymbol{\Gamma}$ matrix is a complex symmetric matrix with Im $\boldsymbol{\Gamma}$ positive definite so that the quadratic phase in the exponent in Eq. (14) has a positive imaginary part that is generating a smooth Gaussian window that is strongest for $\mathbf{x}=0$ and decays as $\mathbf{x}$ in-

creases. The norm of the window is obtained by inserting Eqs. (14) into Eq. (11), giving $\hat{N}^2=\pi/(k_o\Gamma_i)$.

Using the Gaussian windows [Eqs. (14)] in Eq. (13), we obtain the plane-wave spectral representation for the Gaussian beam propagators in $z>0$ half-space,

$$\hat{B}(\mathbf{r};\bar{\mathbf{X}})=\frac{ik_o}{2\pi\Gamma}\int \mathrm{d}^2\xi\,\exp[ik_o\Phi(\mathbf{r},\boldsymbol{\xi},\bar{\boldsymbol{\xi}})], \tag{15}$$

where

$$\Phi(\mathbf{r},\boldsymbol{\xi},\bar{\boldsymbol{\xi}})=\boldsymbol{\xi}\cdot(\mathbf{x}-\bar{\mathbf{x}})+\zeta(\boldsymbol{\xi})z-(\boldsymbol{\xi}-\bar{\boldsymbol{\xi}})^2/(2\Gamma). \tag{16}$$

Equation (15) describes the Gaussian beam propagator in terms of superposition of plane-waves, propagating in the direction of the unit vector $\hat{\boldsymbol{\kappa}}(\boldsymbol{\xi})$ in Eq. (5) away from the initial aperture. This spectral integral cannot be evaluated in closed form for the generic wave-number profile $\zeta(\boldsymbol{\xi})$. Instead, saddle-point asymptotics may be applied for the ordinary (Section 3) and the extraordinary (Section 4) field propagators.

3. ORDINARY GAUSSIAN BEAM PROPAGATORS

In order to compare and contrast the three-dimensional extraordinary with the ordinary GB propagators, we shall briefly discuss in this section the expressions for the latter, which have been derived previously[4] in connection with a homogeneous isotropic medium.

A. Asymptotic Evaluation and Parameterization

In view of Eq. (1), the ordinary wave-number profile is described by [see also Eq. (53)]

$$\zeta(\boldsymbol{\xi})=(1-\boldsymbol{\xi}^2)^{1/2},\quad \mathrm{Im}\,\zeta\geqslant 0. \tag{17}$$

Using the ordinary wave-number profile [Eq. (17)] in Eqs. (15) and (16), we obtain the plane-wave spectral representation of the ordinary GB. The resulting integral cannot be evaluated in closed form. With the saddle-point technique as well as a paraxial approximation, this integral may be evaluated asymptotically.[4] The result is given below. We use the (ordinary) local beam coordinates (x_{b_1},x_{b_2},z_b) defined, for a given phase-space spectral variable $\bar{\boldsymbol{\xi}}$, by the transformation

$$\begin{pmatrix}x_{b_1}\\ x_{b_2}\\ z_b\end{pmatrix}=\begin{bmatrix}\cos\bar{\vartheta}\cos\bar{\varphi} & \cos\bar{\vartheta}\sin\bar{\varphi} & -\sin\bar{\vartheta}\\ -\sin\bar{\varphi} & \cos\bar{\varphi} & 0\\ \sin\bar{\vartheta}\cos\bar{\varphi} & \sin\bar{\vartheta}\sin\bar{\varphi} & \cos\bar{\vartheta}\end{bmatrix}\begin{pmatrix}x_1-\bar{x}_1\\ x_2-\bar{x}_2\\ z\end{pmatrix}, \tag{18}$$

where $(\bar{\vartheta},\bar{\varphi})$ are the spherical angles that define the ordinary beam direction $\hat{\bar{\boldsymbol{\kappa}}}_{\mathrm{iso}}=(\bar{\boldsymbol{\xi}},\bar{\zeta})$, with $\bar{\zeta}=\zeta(\bar{\boldsymbol{\xi}})$. Thus the z_b axis coincides with the beam axis, while the transverse coordinates $\mathbf{x}_b=(x_{b_2},x_{b_1})$ are rotated such that x_{b_1} lies in the plane containing $\bar{\boldsymbol{\xi}}$ and $\hat{\bar{\boldsymbol{\kappa}}}_{\mathrm{iso}}$ and x_{b_2} lies in the $z=0$ plane (see Fig. 1). Using the beam coordinates, we obtain

$$\hat{B}(\mathbf{r};\hat{\bar{\mathbf{X}}})=\left[\frac{\det\boldsymbol{\Gamma}(z_b)}{\det\boldsymbol{\Gamma}(0)}\right]^{1/2}\exp\left[ik_o\left(z_b+\frac{1}{2}\mathbf{x}_b\boldsymbol{\Gamma}(z_b)\mathbf{x}_b^T\right)\right], \tag{19}$$

where det denotes a matrix determinant, and

$$\boldsymbol{\Gamma}(z_b)=\begin{bmatrix}(z_b+\bar{\zeta}^2/\Gamma)^{-1} & 0\\ 0 & (z_b+1/\Gamma)^{-1}\end{bmatrix}. \tag{20}$$

Note that in an exact (asymptotic) beam, the elements of $\boldsymbol{\Gamma}$ depend on z, whereas in a conventional GB the elements of $\boldsymbol{\Gamma}$ depend only on the location along the beam axis (i.e., on z_b). The difference is due to the fact that in the conventional GB, the Gaussian initial conditions are given on a plane normal to the beam axis, whereas here they are defined on a plane of constant z that is generally inclined with respect to the beam axis. For large z_b or near the beam axis, $\hat{B}$ changes smoothly into a conventional GB, where by setting $z\bar{\zeta}^{-1}\simeq z_b$ we obtain the paraxial form in Eq. (19) with Eq. (20) where $\mathbf{x}_b\boldsymbol{\Gamma}\mathbf{x}_b^T=\Gamma_1x_{b1}^2+\Gamma_2x_{b2}^2$, where Γ_i denotes the diagonal (ii) element of $\boldsymbol{\Gamma}$ matrix [i.e., $\boldsymbol{\Gamma}(z_b)=\mathrm{diag}(\Gamma_1,\Gamma_2)$] and $\hat{B}(\mathbf{r};\bar{\mathbf{X}})$ takes the conventional form of a Gaussian beam propagating along the z_b beam axis.

The parameters of this astigmatic BG may be obtained by rewriting the diagonal elements in Eq. (20) in the form $\Gamma_{1,2}(z_b)=(z_b-Z_{1,2}-iF_{1,2})^{-1}$, where

$$Z_1=-\Gamma_r/|\Gamma|^2\bar{\zeta}^2,\quad Z_2=-\Gamma_r/|\Gamma|^2 \tag{21}$$

are identified as the beam waist location in the $(z_b,x_{b_{1,2}})$ planes, respectively, and

$$F_1=\Gamma_i/|\Gamma|^2\bar{\zeta}^2,\quad F_2=\Gamma_i/|\Gamma|^2, \tag{22}$$

are the corresponding collimation lengths. Furthermore, the e^{-1} beam widths in the $(z_b,x_{b_{1,2}})$ cross-sectional planes, $2\sqrt{2}D_{1,2}$, are found from $\mathrm{Re}\,\Gamma(z_b)$, giving

$$D_{1,2}=(F_{1,2}/k_o)^{1/2}[1+(z_b-Z_{1,2})^2/F_{1,2}^2]^{1/2}, \tag{23}$$

and the phase-front radius of curvature $R_{1,2}$ may be obtained from $\mathrm{Im}\,\Gamma(z_b)$, giving

$$R_{1,2}=(z_b-Z_{1,2})+F_{1,2}^2/(z_b-Z_{1,2}). \tag{24}$$

The beam-propagator astigmatism is caused by the beam tilt with respect to the initial $z=0$ plane, which reduces the effective initial beam width in the x_{b_1} direction. Note that the waist locations $Z_{1,2}$ and the collimation lengths $F_{1,2}$, as well as the phase as a whole, are frequency independent. However, the beam widths $D_{1,2}$ are frequency dependent, being proportional to $\omega^{-1/2}$. These properties identify the scattering propagators as "isodiffracting" wave packets.[23]

Asymptotic propagator (19) allows an insight to the role of the paraxial approximation of astigmatic beams for which the initial distribution plane is tilted with respect to the beam axis: paraxially approximated beams do not satisfy the boundary condition $\hat{B}(\mathbf{r};\bar{\mathbf{X}})|_{z=0}=\hat{W}(\mathbf{x};\bar{\mathbf{X}})$, since the paraxial approximation $z_b\gg(x_{b_1}^2+x_{b_2}^2)^{1/2}$ fails near the $z=0$ plane. The paraxially approximated (astigmatic) beam is obtained by projecting the initial window onto the

$z_b=0$ transverse plane over which the initial effective beam width in the x_{b_1} direction is reduced by a factor of $\bar{\zeta}$, whereas the width in the x_{b_2} direction remains unchanged; i.e., the paraxial beam boundary conditions on the plane transverse to the tilted beam axis ($z_b=0$) are

$$\hat{B}(\mathbf{r};\bar{\mathbf{X}})_{z_b=0}=\exp\left(\tfrac{i}{2}k_o\mathbf{x}_b\boldsymbol{\Gamma}_{\text{parax}}\mathbf{x}_b^T\right), \tag{25}$$

with

$$\boldsymbol{\Gamma}_{\text{parax}}=\begin{bmatrix}\Gamma/\bar{\zeta}^2 & 0\\ 0 & \Gamma\end{bmatrix}. \tag{26}$$

For large-angle paraxial parameterization, the use of a nonorthogonal coordinate systyem is required. This novel approach is presented in Section 4 for extraordinary-beam propagators [see Eq. (37)].

B. Phase-Space Localization

The effective domain of integration in Eq. (12) does not include the entire PS domain $(-\infty,\infty)$ owing to the *a priori* localization in the phase space around well-defined regions in the $\bar{\mathbf{X}}$ domain. Owing to the Gaussian decay of the beam propagators $\hat{B}(\mathbf{r};\bar{\mathbf{X}})$, away from the beam axis, only beams that pass near a given observation point $\mathbf{r}$ actually contribute to the field. For a given observation point $\mathbf{r}$, this localizes the contributions in Eq. (12) to the vicinity of a hyperplane in the $\bar{\mathbf{X}}$ domain, defined for ordinary-mode beams by

$$(\mathbf{x}-\bar{\mathbf{x}})/\bar{R}=\bar{\boldsymbol{\xi}},\quad \bar{R}\equiv(|\mathbf{x}-\bar{\mathbf{x}}|^2+z^2)^{1/2}. \tag{27}$$

This (ordinary) observation manifold defines the phase-space beams that pass through $\mathbf{r}$ [compare with the extraordinary manifold in Eq. (50)].

4. EXTRAORDINARY GAUSSIAN BEAM PROPAGATORS

For extraordinary modes, for which the wave-number profiles are given by the generic form of Eq. (1), beam propagators (15) may be evaluated asymptotically in the high-frequency regime by applying localization considerations to the generic medium characteristics.

A. Asymptotic Evaluation and Parametrization

The stationary point $\boldsymbol{\xi}_s$ of phase (16) satisfies

$$\nabla\Phi\,|_{\boldsymbol{\xi}=\boldsymbol{\xi}_s}=\mathbf{x}-\bar{\mathbf{x}}+z\,\nabla\zeta\,|_{\boldsymbol{\xi}=\boldsymbol{\xi}_s}-|\boldsymbol{\xi}_s-\bar{\boldsymbol{\xi}}|/\Gamma=0, \tag{28}$$

where $\nabla=(\partial_{\xi_1},\partial_{\xi_2})$ and $|\boldsymbol{\xi}_s-\bar{\boldsymbol{\xi}}|=[(\boldsymbol{\xi}_s-\bar{\boldsymbol{\xi}})\cdot(\boldsymbol{\xi}_s-\bar{\boldsymbol{\xi}})]^{1/2}$. Equation (28) has a real solution only if $\boldsymbol{\xi}_s=\bar{\boldsymbol{\xi}}$ for $\bar{\boldsymbol{\xi}}$ in the propagating region [where $\zeta(\bar{\boldsymbol{\xi}})$ is real] and only for observation points that satisfy

$$\mathbf{x}-\bar{\mathbf{x}}+\nabla\bar{\zeta}z=0, \tag{29}$$

where, here and henceforth, bar over ζ denotes sampling at $\boldsymbol{\xi}=\bar{\boldsymbol{\xi}}$ (i.e., $\bar{\zeta}=\zeta(\bar{\xi})$, $\nabla\bar{\zeta}\equiv\nabla\zeta(\boldsymbol{\xi})|_{\boldsymbol{\xi}=\bar{\boldsymbol{\xi}}}$, etc.). Condition (29) defines the beam axis as being a tilted line in the configuration space, with an anisotropy-dependent tilt. Therefore the beam axis is directed along the unit vector

$$\hat{\bar{\boldsymbol{\kappa}}}(\bar{\boldsymbol{\xi}})=(\cos\bar{\vartheta}_1,\cos\bar{\vartheta}_2,\cos\bar{\vartheta}), \tag{30}$$

where $\bar{\vartheta}$ is the angle with respect to the z axis and $\bar{\vartheta}_{1,2}$, are the beam-axis angles with respect to the (x_1,x_2) axes, respectively. In view of Eq. (29), $\vartheta_{1,2}$ are given by

$$\cos\bar{\vartheta}_{1,2}=-\cos\bar{\vartheta}\partial_{\xi_{1,2}}\bar{\zeta},\quad \cos\bar{\vartheta}=(|\nabla\bar{\zeta}|^2+1)^{-1/2}. \tag{31}$$

Note that for the ordinary (isotropic) case, in which ζ is given by Eq. (17), the beam direction in Eq. (30) coincides with $\hat{\bar{\boldsymbol{\kappa}}}=(\bar{\boldsymbol{\xi}},\bar{\zeta})$ in Eq. (18). The beam axis direction (30) is directly related to the wave-number surface $\zeta(\boldsymbol{\xi})$ over the (ξ_1,ξ_2) plane: Since $\cos\bar{\vartheta}_{1,2}$ are proportional to the gradient of the surface at $\bar{\boldsymbol{\xi}}$, it follows that the beam axis $\hat{\bar{\boldsymbol{\kappa}}}$ is in the direction of the *normal to the wave-number surface* at the on-axis stationary point $\bar{\boldsymbol{\xi}}$ (see Fig. 2).

For *off-axis observation points*, Eq. (28) could not be solved explicitly. Furthermore, the off-axis stationary point is complex, and the solution requires analytic continuation of the wave-number profile $\zeta(\boldsymbol{\xi})$ for complex $\boldsymbol{\xi}$. To allow us to obtain a closed-form analytic solution for the beam field, we notice that the beam field decays away from the beam axis. Therefore we may apply a Taylor expansion of the phase [Eq. (16)] about the on-axis stationary point $\boldsymbol{\xi}_s=\bar{\boldsymbol{\xi}}$,

$$\Phi(\boldsymbol{\xi})\approx\Phi_0+\boldsymbol{\Phi}_1(\boldsymbol{\xi}-\bar{\boldsymbol{\xi}})^T+\tfrac{1}{2}(\boldsymbol{\xi}-\bar{\boldsymbol{\xi}})\boldsymbol{\Phi}_2(\boldsymbol{\xi}-\bar{\boldsymbol{\xi}})^T, \tag{32}$$

with

$$\Phi_0=\Phi(\bar{\boldsymbol{\xi}})=\bar{\boldsymbol{\xi}}\cdot(\mathbf{x}-\bar{\mathbf{x}})+\bar{\zeta}z,\quad \boldsymbol{\Phi}_1=(\mathbf{x}-\bar{\mathbf{x}})+\nabla\bar{\zeta}z, \tag{33}$$

$$\boldsymbol{\Phi}_2=\begin{bmatrix}-1/\Gamma+\partial^2_{\xi_1}\bar{\zeta}z & \partial^2_{\xi_1\xi_2}\bar{\zeta}z\\ \partial^2_{\xi_1\xi_2}\bar{\zeta}z & -1/\Gamma+\partial^2_{\xi_2}\bar{\zeta}z\end{bmatrix}. \tag{34}$$

Using Eq. (32), one finds that the saddle point for both on- and off-axis observation points is $\boldsymbol{\xi}_s=\bar{\boldsymbol{\xi}}-\boldsymbol{\Phi}_2^{-1}\boldsymbol{\Phi}_1$, and the field in Eq. (15) may be evaluated asymptotically by

$$\hat{B}(\mathbf{r};\bar{\mathbf{X}})=\frac{i/\Gamma}{\sqrt{-\det\boldsymbol{\Phi}_2}}\exp[ik_oS(\mathbf{r})],$$

$$S(\mathbf{r})=\Phi_0-1/2\boldsymbol{\Phi}_1\boldsymbol{\Phi}_2^{-1}\boldsymbol{\Phi}_1^T. \tag{35}$$

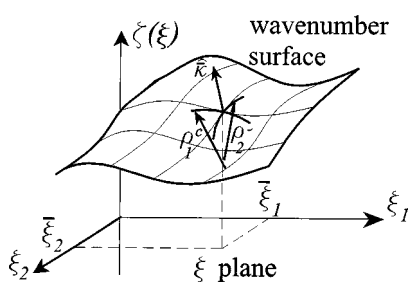

Fig. 2. Wave-number surface and parameterization. The parameterization of the beam propagators is matched to local geometrical properties of the wave-number surface $\zeta(\boldsymbol{\xi})$ at the the processing point $\boldsymbol{\xi}=\bar{\boldsymbol{\xi}}$: the normal $\hat{\bar{\boldsymbol{\kappa}}}$ and the radii of curvature along constant ξ_1 or ξ_2, $\rho^c_{1,2}$, of the surface.

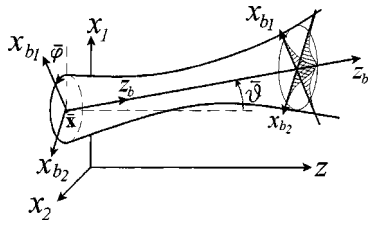

Fig. 3. Local beam coordinate frame for the extraordinary GB propagator. The beam axis is directed along the unit vector $\hat{\bar{\boldsymbol{\kappa}}}$. The local transverse coordinates $\mathbf{x}_b$ are given by transformation (36) so that the GB [Eq. (40)] exhibits quadratic Gaussian decay in the local $\mathbf{x}_b$ coordinates.

In a manner similar to that for the ordinary beam [see Eq. (18)], the beam field in Eqs. (35) may be presented in terms of (anisotropic) local beam coordinates over which the field exhibits a Gaussian decay away from the beam axis. We define the local beam coordinates $\mathbf{r}_b=(x_{b1},x_{b2},z_b)$ by the nonorthogonal transformation

$$\begin{pmatrix} x_{b_1} \\ x_{b_2} \\ z_b \end{pmatrix} = \mathbf{T}\begin{pmatrix} x_1-\bar{x}_1 \\ x_2-\bar{x}_2 \\ z \end{pmatrix}, \tag{36}$$

where the transformation matrix $\mathbf{T}$ is given by

$$\mathbf{T}=\begin{bmatrix} \cos\bar{\varphi} & \sin\bar{\varphi} & (-\cos\bar{\vartheta}_2\sin\bar{\varphi}-\cos\bar{\vartheta}_1\cos\bar{\varphi})/\cos\bar{\vartheta} \\ -\sin\bar{\varphi} & \cos\bar{\varphi} & (-\cos\bar{\vartheta}_2\cos\bar{\varphi}+\cos\bar{\vartheta}_1\sin\bar{\varphi})/\cos\bar{\vartheta} \\ 0 & 0 & 1/\cos\bar{\vartheta} \end{bmatrix}, \tag{37}$$

where $\cos\bar{\vartheta}_{1,2,3}$ are defined in Eqs. (31) and the angle $\bar{\varphi}$ is defined by

$$\tan 2\bar{\varphi}=-2\partial^2_{\xi_1\xi_2}\bar{\zeta}/(\partial^2_{\xi_2}\bar{\zeta}-\partial^2_{\xi_1}\bar{\zeta}). \tag{38}$$

Transformation (37) consists of a rotation transformation in the (x_1,x_2) plane by $\bar{\varphi}$, for which the phase $S(\mathbf{r})$ in Eqs. (35) exhibits Gaussian decay, followed by tilting of the z axis toward the beam-axis direction in Eq. (30) (see Fig. 3). The inverse transform is given by

$$\mathbf{T}^{-1}=\begin{bmatrix} \cos\bar{\varphi} & -\sin\bar{\varphi} & \cos\bar{\vartheta}_1 \\ \sin\bar{\varphi} & \cos\bar{\varphi} & \cos\bar{\vartheta}_2 \\ 0 & 0 & \cos\bar{\vartheta} \end{bmatrix}. \tag{39}$$

With the beam coordinate system (36) in Eqs. (35), the field may be presented in Gaussian quadratic form,

$$\hat{B}(\mathbf{r};\bar{\mathbf{X}})=\left[\frac{\det\boldsymbol{\Gamma}(z_b)}{\det\boldsymbol{\Gamma}(0)}\right]^{1/2}\exp\left[ik_o\left(\hat{\bar{\boldsymbol{\kappa}}}_{\rm iso}\cdot[\mathbf{r}-(\bar{\mathbf{x}},0)]+\frac{1}{2}\mathrm{x}_b\boldsymbol{\Gamma}(z_b)\mathbf{x}_b^T\right)\right], \tag{40}$$

where det denotes a matrix determinant, $\hat{\bar{\boldsymbol{\kappa}}}_{\rm iso}=(\bar{\boldsymbol{\xi}},\bar{\zeta})$ and $\boldsymbol{\Gamma}(z_b)=\mathrm{diag}(\Gamma_1,\Gamma_2)$ is a symmetric matrix whose diagonal elements $\Gamma_{1,2}(z)$, are given by

$$\Gamma_{1,2}(z)=\left(1/\Gamma-z\frac{1}{2}\left\{\partial^2_{\xi_1}\bar{\zeta}+\partial^2_{\xi_2}\bar{\zeta}\mp[(\partial^2_{\xi_1}\bar{\zeta}-\partial^2_{\xi_2}\bar{\zeta})^2+4(\partial^2_{\xi_1\xi_2}\bar{\zeta})^2]^{1/2}\right\}\right)^{-1}. \tag{41}$$

Note that the linear term of the phase in Eq. (40) is $\hat{\bar{\boldsymbol{\kappa}}}_{\rm iso}\cdot[\mathbf{r}-(\bar{\mathbf{x}},0)]$; that is, the phase is accumulated along the unit vector $(\bar{\boldsymbol{\xi}},\bar{\zeta})$, which is in general different from the beam-axis direction $\hat{\bar{\boldsymbol{\kappa}}}$ in Eq. (30). For ordinary beams, where $\zeta(\boldsymbol{\xi})$ is given by Eq. (17), the two vectors coincide, thereby setting $\hat{\bar{\boldsymbol{\kappa}}}_{\rm iso}\cdot[\mathbf{r}-(\mathbf{x},0)]=z_b$ as in Eq. (19).

Using Eq. (38) in Eq. (41), we may rewrite $\Gamma_{1,2}$ in the form $\Gamma_{1,2}(z_b)=(z_b a_{1,2}+1/\Gamma)^{-1}$, where

$$a_{1,2}=\begin{Bmatrix}-\\+\end{Bmatrix}\frac{\cos\bar{\vartheta}}{\cos(2\bar{\varphi})}\left[\partial^2_{\xi_1}\bar{\zeta}\begin{Bmatrix}\cos^2\bar{\varphi}\\ \sin^2\bar{\varphi}\end{Bmatrix}-\partial^2_{\xi_2}\bar{\zeta}\begin{Bmatrix}\sin^2\bar{\varphi}\\ \cos^2\bar{\varphi}\end{Bmatrix}\right]. \tag{42}$$

In order to relate the beam field to local geometrical properties of the wave-number surface $\zeta(\boldsymbol{\xi})$, we denote $\rho^c_{1,2}$ as the radii of curvature of the curves $\zeta(\boldsymbol{\xi})|_{\xi_{1,2}=\bar{\xi}_{1,2}}$, i.e., of the wave-number surface cross-sectional planes of constant ξ_1 or ξ_2, respectively, that pass through the on-axis stationary point $\bar{\boldsymbol{\xi}}$ (see Fig. 2):

$$\rho^c_{1,2}=\frac{[1+(\partial_{\xi_{1,2}}\bar{\zeta})^2]^{3/2}}{\partial^2_{\xi_{1,2}}\bar{\zeta}}. \tag{43}$$

By inserting Eqs. (31) into (43), we obtain

$$\partial^2_{\xi_{1,2}}\bar{\zeta}=\left(\frac{\sin\vartheta_{2,1}}{\cos\vartheta_3}\right)^3\frac{1}{\rho^c_{1,2}}, \tag{44}$$

and relation (42) may be writen in the form

$$a_{1,2}=\begin{Bmatrix}-\\+\end{Bmatrix}\frac{\cos^{-2}\bar{\vartheta}}{\cos(2\bar{\varphi})}\left[\frac{\sin^3\vartheta_2}{\rho^c_1}\begin{Bmatrix}\cos^2\bar{\varphi}\\ \sin^2\bar{\varphi}\end{Bmatrix}-\frac{\sin^3\vartheta_1}{\rho^c_2}\begin{Bmatrix}\sin^2\bar{\varphi}\\ \cos^2\bar{\varphi}\end{Bmatrix}\right]. \tag{45}$$

We may carry out the parameterization of the anisotropic beam propagator in a manner similar to that for the isotropic beam in Eq. (19), rewriting $\Gamma_{1,2}=[a_{1,2}(z_b-Z_{1,2}-iF_{1,2})]^{-1}$, where

$$Z_{1,2}=-\Gamma_r/(|\Gamma|^2a_{1,2}),\quad F_{1,2}=\Gamma_i/(|\Gamma|^2a_{1,2}) \tag{46}$$

are identified as the beam waist location in the $(z_b,x_{b_{1,2}})$ plane and the corresponding collimation length, respectively. Furthermore, by rewriting

$$\Gamma_{1,2}(z_b)=\frac{1}{R_{1,2}(z_b)}+\frac{i}{k_oD^2_{1,2}(z_b)}, \tag{47}$$

we identify $2\sqrt{2}D_{1,2}$ where

$$D_{1,2}(z_b)=(F_{1,2}a_{1,2}/k_o)^{1/2}[1+(z_b-Z_{1,2})^2/F^2_{1,2}]^{1/2} \tag{48}$$

as the e^{-1} beam width in the $(z_b,x_{b_{1,2}})$ plane, and

$$R_{1,2}(z_b)=a_{1,2}[(z_b-Z_{1,2})+F^2_{1,2}/(z_b-Z_{1,2})] \tag{49}$$

is the phase-front radius of curvature. The resulting GB is therefore astigmatic (having $Z_1\neq Z_2$). This astigmatism

is caused by the beam tilt, which reduces the effective initial beam width in the $x_{b_{1,2}}$ directions.

The compact presentation in Eqs. (45)–(49) parameterizes the GB field in terms of local properties of the generic wave-number profile about the PS (directional) parameter $\boldsymbol{\xi}=\bar{\boldsymbol{\xi}}$. The parameter $a_{1,2}$ in Eq. (45), which parameterizes the anisotropy effect on the beam parameters in Eqs. (46)–(49), is affected by the geometrical properties of the wave-number surface $\zeta(\boldsymbol{\xi})$: The angles $\vartheta_{1,2}$ are determined by the normal of the surface at $\bar{\boldsymbol{\xi}}$, and $\rho^c_{1,2}$ are the radii of curvatures at that point.

B. Phase-Space Localization

The effective domain of integration in phase-space representation (12) of the ordinary field is limited because of the observation manifold in which the $\bar{\mathbf{X}}$ integration is limited to the vicinity of a hyperplane in Eq. (27). For extraordinary-mode propagation, the beam-axis direction in Eq. (30) sets the observation manifold to

$$(\mathbf{x}-\bar{\mathbf{x}})/\bar{R}=\cos\bar{\vartheta}_{1,2},\quad \bar{R}\equiv(|\mathbf{x}-\bar{\mathbf{x}}|^2+z^2)^{1/2}, \tag{50}$$

where $\bar{\vartheta}_{1,2}$ in Eqs. (31) are determined by the phase-space parameter $\bar{\mathbf{X}}$ as well as the normal to wave-number profile, $\nabla\zeta(\boldsymbol{\xi})$, at $\bar{\boldsymbol{\xi}}$. Therefore the contributing hyperplane is obtained by matching observation angles to those of the wave-number surface normals.

5. ILLUSTRATIVE EXAMPLE

The general results for the beam propagators in the generic anisotropic wave-number profile are tested here for the special case of the electromagnetic wave-number profile of a uniaxial crystal identified by the dielectric tensor

$$\boldsymbol{\epsilon}_r=\begin{bmatrix}\epsilon & 0 & 0\\ 0 & \epsilon & 0\\ 0 & 0 & \epsilon_z\end{bmatrix}. \tag{51}$$

The uniaxial crystal wave-number profiles satisfy Fresnel's equation[24]

$$\frac{k_{x_1}^2}{c^2(k)-c_x^2}+\frac{k_{x_2}^2}{c^2(k)-c_x^2}+\frac{k_z^2}{c^2(k)-c_z^2}=0,$$

$$c(k)=\omega/(k_{x_1}^2+k_{x_2}^2+k_z^2)^{1/2}, \tag{52}$$

where $c_x=c_0/\sqrt{\epsilon}$, $c_z=c_0/\sqrt{\epsilon_z}$, with c_0 being the speed of light *in vacuo*, are called the principal phase velocities of the crystal.

Solving Eqs. (52) for k_z and using the normalization in Eq. (1) where we choose $c=c_x$, we find two solutions: the ordinary mode, where

$$\zeta(\boldsymbol{\xi})=(1-\xi_2^2-\xi_1^2)^{1/2}, \tag{53}$$

and the extraordinary propagation mode, where

$$\zeta(\boldsymbol{\xi})=(1-(\xi_2^2+\xi_1^2)/\epsilon_z)^{1/2}. \tag{54}$$

To illustrate the beam parametrization, we shall proceed by using extraordinary propagation profile (54) with $\bar{\boldsymbol{\xi}}\neq 0$, so that the beam is propagating with some angle with respect to the crystal axis of symmetry.

The beam propagators may be evaluated numerically by using exact plane-wave spectral representation (13) for the Gaussian window plane-wave distribution in Eqs. (14). In the following examples, this integral is evaluated numerically for wave-number profile (54) and is referred to as the reference solution to which the asymptotic beam field and parameterization are compared. All simulations are carried out for $\Gamma_{1,2}=-1+i$, $\bar{\xi}_1=0.1$, $\bar{\xi}_2=0.3$, $\bar{\mathbf{x}}=0$, $k=800\ \mathrm{m}^{-1}$, $\epsilon=1$, and $\epsilon_z=1.3$.

A. Gaussian Beam Amplitude Contour Plots

Figure 4 depicts the reference solution for the astigmatic Gaussian beam amplitude ($|\hat{B}|$) contour plots over the $z=1$ plane. Contour levels are at $(e^{-1/2},e^{-1},e^{-2})$ with respect to the beam peak amplitude at $\mathbf{x}_b=0$. The local beam transverse coordinates, x_{b_1}, x_{b_2} are depicted over the (x_1,x_2) plane. The rotation transform of (x_1,x_2) to (x_{b_1},x_{b_2}) by $\bar{\varphi}=-10.4°$ in Eq. (38) is carried out so that the resulting field Eq. (40) exhibits quadratic Gaussian decay in the local coordinates, as can be seen clearly in the figure. The circles denotes the beam widths over the $x_{b_{1,2}}$ axes $D_{1,2}$, evaluated according to Eq. (48) for wave-number profile (54), and they match the reference solution contour of $e^{-1/2}$.

B. Astigmatism and Waist Location

To demonstrate the beam tilting and astigmatism, the asymptotic beam $e^{-1/2}$ contours in the $(x_{b_{1,2}},z)$ cross-sectional planes are plotted in Figs. 5(a) and 5(b), respectively. The waist location [Eqs. (46)] is marked by a circle

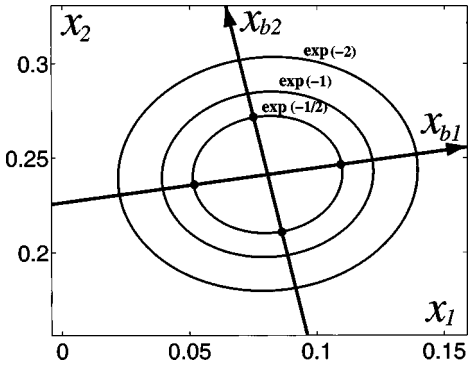

Fig. 4. Gaussian beam amplitude contour plots over $z=1$ plane for the reference solution evaluated by using exact plane-wave spectral representation (13).

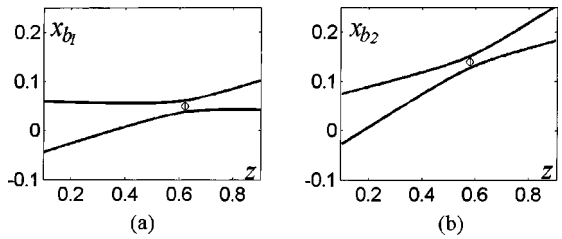

Fig. 5. Astigmatism and waist location; the asymptotic beam $\exp(-1/2)$ contours in the $(x_{b_{1,2}},z)$ planes are shown in (a) and (b), respectively, as well as the waist location (circle) and the beam width (vertical line) in each plot.

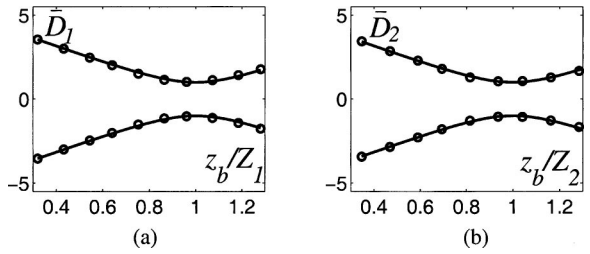

Fig. 6. Beam width in the local transverse coordinates. Solid curves plot the asymptotic-beam widths (48), $D_{1,2}(z_b)$, and circles plot the reference field exp(−1/2) contours in (a) and (b) for the $(x_{b_{1,2}},z_b)$ planes, respectively.

over the beam axis along with the beam width [Eq. (48)]at the waists (vertical solid line). Note that the the beam-waist locations are different in Figs. 5(a) and 5(b).

C. Beam Width in the Local Transverse Coordinates

To compare the asymptotic-beam widths $D_{1,2}(z_b)$ in Eq. (48) with the reference solution, the latter was evaluated over the $(x_{b_{1,2}},z_b)$ planes, and the resulting $e^{-1/2}$ contours are plotted with circles in Figs. 6(a) and 6(b), respectively; the solid curves are the analytic beam width in Eq. (48). For both graphs, the longitudinal coordinate z_b is scaled with respect to the beam waist location at $z_b=Z_{1,2}$, and the widths were scaled with respect to the corresponding beam width at the waists. The figure clearly demonstrates a good agreement between the reference solution and the asymptotic parameterization.

6. CONCLUSION

In this paper we have been concerned with field propagation in an anisotropic medium characterized by a generic wave-number profile. Using a local (windowed) transform, we presented the initial field at $z=0$ as a superposition of Gaussian window functions that are located in each point $\bar{\mathbf{x}}$ in the aperture, with linear $\bar{\boldsymbol{\xi}}$ phases. For each window function, a propagation solution in $z>0$ was found by using saddle-point approximation. The resulting beam-propagator characteristics were analytically parameterized in terms of wave-number profile characteristics at PS processing parameter $\bar{\boldsymbol{\xi}}$. The analytic results and the numeric results for a specific wave-number profile of extraordinary mode in uniaxial crystal were compared and were found to conform remarkably well. A local spectral representation for time-dependent fields is presented in a companion paper.[8]

ACKNOWLEDGMENT

This research was supported by a grant from the G.I.F., The German-Israeli Foundation for Scientific Research and Development.

Timor Melamed can be reached at timormel @ee.bgu.ac.il.

REFERENCES

1. M. J. Bastiaans, "The expansion of an optical signal into a discrete set of Gaussian beams," Optik (Stuttgart) **57**, 95–102 (1980).
2. B. Z. Steinberg, E. Heyman, and L. B. Felsen, "Phase-space beam summation for time-harmonic radiation from large apertures," J. Opt. Soc. Am. A **8**, 41–59 (1991).
3. A. Dendane and J. M. Arnold, "Scattered field analysis of a focused reflector using the Gabor series," IEE Proc. Part H Microwaves, Antennas Propag. **141**, 216–222 (1994).
4. T. Melamed, "Phase-space beam summation: a local spectrum analysis for time-dependent radiation," J. Electromagn. Waves Appl. **11**, 739–773 (1997).
5. J. M. Arnold, "Phase-space localization and discrete representations of wave fields," J. Opt. Soc. Am. A **12**, 111–123 (1995).
6. J. M. Arnold and L. B. Felsen, "Rays, beams and diffraction in a discrete phase space: Wilson bases," Opt. Express **10**, 716–727 (2002).
7. D. Lugaraand, C. Letrou, A. Shlivinski, E. Heyman, and A. Boag, "Frame-based Gaussian beam summation method: theory and applications," Radio Sci. **38**, 1–15 (2003).
8. I. Tinkelman and T. Melamed, "Local spectrum analysis of field propagation in anisotropic media. Part II. Time-dependent fields," J. Opt. Soc. Am. A **22** 1208–1215 (2005).
9. C. Yangjian, L. Qiang, and G. Di, "Propagation of partially coherent twisted anisotropic Gaussian Schell-model beams in dispersive and absorbing media," J. Opt. Soc. Am. A **19**, 2036–2042 (2002).
10. L. I. Perez and M. T. Garea, "Propagation of 2D and 3D Gaussian beams in an anisotropic uniaxial medium: vectorial and scalar treatment," Optik (Stuttgart) **111**, 297–306 (2000).
11. E. Poli, G. V. Pereverzev, and A. G. Peeters, "Paraxial Gaussian wave beam propagation in an anisotropic inhomogeneous plasma," Phys. Plasmas **6**, 5–11 (1999).
12. R. Simon and N. Mukunda, "Shape-invariant anisotropic Gaussian Schell-model beams: a complete characterization," J. Opt. Soc. Am. A **15**, 1361–1370 (1998).
13. X. B. Wu and R. Wei, "Scattering of a Gaussian beam by an anisotropic material coated conducting circular cylinder," Radio Sci. **30**, 403–411 (1995).
14. A. Hanyga, "Gaussian beams in anisotropic elastic media," Geophys. J. R. Astron. Soc. **85**, 473–503 (1986).
15. K. Sundar, N. Mukunda, and R. Simon, "Coherent-mode decomposition of general anisotropic Gaussian Schell-model beams," J. Opt. Soc. Am. A **12**, 560–569 (1995).
16. M. Spies, "Modeling of transducer fields in inhomogeneous anisotropic materials using Gaussian beam superposition," Nondestr. Test. Eval. Int. **33**, 155–162 (2000).
17. S. Y. Shin and L. B. Felsen, "Gaussian beams in anisotropic media," Appl. Phys. **5**, 239–250 (1974).
18. I. Tinkelman and T. Melamed, "Gaussian beam propagation in generic anisotropic wave-number profiles," Opt. Lett. **28**, 1081–1083 (2003).
19. L. B. Felsen and N. Marcuvitz, *Radiation and Scattering of Waves* (IEEE Press, Piscataway, N.J., 1994).
20. P. C. Clemmow, *The Plane Wave Spectrum Representation of Electromagnetic Fields* (IEEE Press, Piscataway, N.J., 1996).
21. M. M. Popov V. Červeny, and I. Pšenčik, "Computation of wave fields in inhomogeneous media—Gaussian beam approach," Geophys. J. R. Astron. Soc. **70**, 109–128 (1982).
22. E. Heyman, "Pulsed beam propagation in an inhomogeneous medium," IEEE Trans. Antennas Propag. **42**, 311–319 (1994).
23. E. Heyman and T. Melamed, "Certain considerations in aperture synthesis of ultrawideband/short-pulse radiation," IEEE Trans. Antennas Propag. **42**, 518–525 (1994).
24. M. Born and E. Wolf, *Principles of Optics* (Pergamon, New York, 1964).